Am J Transl Res 2019;11(10):6356-6369
www.ajtr.org /ISSN:1943-8141/AJTR0094462

Original Article

Pterostilbene attenuates amyloid-β induced neurotoxicity with regulating PDE4A-CREB-BDNF pathway

Jiao Meng[1*], Yuhua Chen[1,2*], Fangfang Bi[1,2], Hua Li[2], Cuicui Chang[1], Wei Liu[2]

[1]Central Laboratory of Medicine School, Xi'an Peihua University, Xi'an 710100, China; [2]Department of Medical Science Research Center, Shaanxi Fourth People's Hospital, Xi'an 710143, China. [*]Equal contributors and co-first authors.

Received March 27, 2019; Accepted July 6, 2019; Epub October 15, 2019; Published October 30, 2019

Abstract: Amyloid-β (Aβ) is considered partially responsible for cognitive dysfunction in Alzheimer's disease (AD). Resveratrol is known as an anti-neurotoxicity potential natural product, however low blood-brain-barrier (BBB) permissibility and low oral-bioavailability (OB) are the main limitations on its clinical potential. In this study, we illustrated that Pterostilbene (PTS), a kind of resveratrol analog which showed higher scores on BBB and OB, could overcome Aβ-induced neurotoxicity *in vitro* and *in vivo*. *In silico* simulation indicated PTS binding with PDE4A may contribute to its anti-apoptosis and anti-neurotoxicity effects. Behavioral tests further confirmed PTS' potential of overcoming memory deficits in APP/PS1 mice (AD model). Interestingly, PTS also rescued the reducing in dendritic spine density in APP/PS1 mice based on Golgi-Cox staining. Besides, as results of reversing Aβ-induced decreases in cyclic-AMP level, PTS increased the pVASP, pCREB, BDNF, and PSD95 expression. Overall, PTS protects neurons against Aβ-induced neurotoxicity and cognitive dysfunction through regulating the PDE4A-CREB-BDNF pathway. Therefore, targeting on PDE4A, PTS would be a qualified natural product for alleviating Aβ-induced neurotoxicity in AD.

Keywords: Pterostilbene, Alzheimer's disease, memory deficit, PDE4A, amyloid-β

Introduction

With an ever-increasing population, the incidence of Alzheimer's disease (AD) in the United States will increase from the current population of 4 million to 14 million in 2050 [1]. Although various efforts have been made to reveal the molecular basis of this chronic disease, little advancement has been made in affirming the pathogenesis. Among the varied hypotheses, amyloid-β (Aβ) hypothesis may be the most acceptable interpretation of AD pathology. Since none of the therapy strategy directly targeting Aβ presents a convincing result on clinical trial [2], discovering novel targets to overcome Aβ-induced neurotoxicity is very urgent for AD therapy.

Phosphodiesterase (PDE) has been reported to be a valuable drug target in many diseases, such as Parkinson's disease [3] and AD [4]. Among 11 subtypes in PDE superfamily, PDE4 and PDE2 are two members involved in neurodegeneration disease [5]. PDE4A and PDE4D are the most studied PDE4 variants [6], as well as PDE2A3 in PDE2 family [7]. PDE4 specially dehydrates cyclic adenosine monophosphate (cAMP) but not cyclic guanosine monophosphate (cGMP), while PDE2 targets on both of the cyclic nucleotides [8]. Studies have shown that they also affect the neuronal cell survival, and may be invovled in neurodegenerative processes when functioning incorrectly [9]. cAMP response element binding protein (CREB) is one of the critical targets of cAMP and cGMP in neuronal signaling [10, 11]. Studies have shown that CREB is associated with up-regulation of growth factors, neurotransmitters, and other signaling molecules which have important roles in neuroplasticity and neuronal survival [5]. *In vitro*, elevated cAMP can rapidly recruit tyrosine-kinase B (TrkB) receptors, which are the

major receptors of brain-derived neurotrophic factor (BDNF), thus enhancing the response to these neurotrophic factors, which is vital for neuronal growth and survival [12]. As a major activator of CREB, down-regulation of AC/cAMP/PKA signaling can also explain the loss of synaptic plasticity and memory loss in AD [13].

In these years, many studies have confirmed Resveratrol' neuroprotective effects on AD in several models, both *in vivo* and *in vitro*. However, the effects of Resveratrol are limited due to its low oral-bioavailability (OB) [14]. Compare to Resveratrol, its structural analog Pterostilbene (PTS) presents higher blood-brain-barrier (BBB) permeability and OB (data collected in TCMSP database). PTS is a phenolic compound originally extracted from sandalwood and later found in fruits such as blueberries and grapes, which are beneficial for neuronal function and cognition during aging [15]. Several studies have demonstrated PTS' effects on Aβ-induced neurotoxicity *in vivo* and *in vitro* [16-18], however, its target protein or signal pathway has not been fully revealed. In this study, we predicted a new target of PTS, PDE4A, and illustrated that PTS overcome Aβ caused neurotoxicity *in vivo* and *in vitro* through PDE4A-CREB-BDNF pathway.

Material and methods

Animals

Eight-month-old male APP/PS1 transgenic mice and littermate wild-type (WT) C57BL/6 mice were purchased from the Cyagen Biosciences (Guangzhou, China). Mice were housed with ambient temperature and humidity controlled to 25°C and 50%, and 12 h of light/dark cycles. Each mouse was allowed to adapt to the environment for 5 days before any treatment. All animal experiments were performed according to the NIH Guide for the Care and Use of Laboratory Animals and approved by the Institutional Animal Care and Use Committee of the Shaanxi Fourth People's Hospital (China).

Drug treatments

$A\beta_{25-35}$ (ab120480) and PKG inhibitor KT5823 (ab120423) were purchased from Abcam company. PTS (4-[(E)-2-(3,5-Dimethoxyphenyl)ethenyl]phenol), Rolipram (4-(3-cyclopentyloxy-4-methoxyphenyl)pyrrolidin-2-one) were obtained from Sigma-Aldrich (St. Louis, MO, USA). PKA inhibitor H89 (S1582) was purchased from Selleck company (Shanghai, China). PTS (5, 10, 20 mg/kg, *p.o.*) was orally administrated constantly once per day for 13 days. Rolipram was dissolved in 0.5% dimethyl sulfoxide (DMSO) and was administrated 30 minutes before the behavioral tests. H89 (1 μL, 5 nmol) and KT-5823 (1 μL, 2 nmol) were administered 30 minutes ahead of PTS or Rolipram treatment. Daniela. Puzzo et al. reviewed the AD rodent models and described the APP/PS1 mice as exhibiting short-term memory deficit, long-term memory deficit, basal synaptic transmission and Aβ pathology from age of 3 months, 6 months, 6 months and 3 months, respectively [19]. We used 8-month APP/PS1 transgenic mice that presented learning and memory impairment by behavioral tests.

Pharmacokinetic comparison

The pharmacological parameters of PTS and Resveratrol were searched from Traditional Chinese Medicine System Pharmacology Database and Analysis Platform (TCMSP, available online: http://lsp.nwsuaf.edu.cn/tcmsp.php), or in ingredient chemical database, respectively. BBB permeability, OB, drug-likeness (DL) evaluation and Caco-2 permeability were selected for comparison. In the TCmsp database, the BBB parameter is defined as NO BBB permeability when BBB < -0.3, partial BBB permeability when -0.3 < BBB < 0.3, high BBB permeability when BBB > 0.3. When searching in the TCMSP database, we set the BBB parameter as BBB > 0.3. Here, OBioavail 1.1, a reliable *in silico* model [20], was used to calculate the OB of structurally diverse drugs and drug-like compounds. Since there is often a good correlation between the absorption of human oral drugs and their apparent permeability coefficients in human intestinal epithelial (Caco-2) cells. Caco-2 cell monolayers are commonly used to predict the fraction of oral dose absorbed and compound's intestinal absorption. In the TCMSP database, the founders calculate the Caco-2 permeability model based on 100 drug compounds and displays an optimal statistical result (R^2 > 0.8). Considering that the compound having Caco-2 < -0.4 is impermeable, the threshold of Caco-2 permeability is set to -0.4.

Docking and molecular dynamics simulation assays

Following Yilixiati Xiaokaiti's assay [21], the molecular docking and molecular dynamics simulation (MD) were briefly described as bellow, CDOCKER algorithm in Discovery Studio (DS) 2.5 (Accelrys Software Inc., San Diego, CA) was used to evaluate the potential molecular binding mode between PTS and PDE4A, PDE4D or PDE2A proteins in this study. Dell optiplex755 server was used to run the program (Round Rock, TX). The crystal structure of PDE4A (PDE4A, PDB ID: 3I8V), PDE4D (PDE4D, PDB ID: 4W1O) and PDE2A (PDE2A, PDB ID: 4D08) were obtained from Protein Data Bank (http://www.rcsb.org/pdb/). The protein was refined with CHARMm after the water molecules in the protein were removed, PTS was docked into the proteins at the same binding site as the internal ligand with proper parameter setting, respectively. Starting from PTS configuration, a set of 10 different orientations were randomly generated. Once the ligand has been docked into the active site, a molecular dynamics (MD) simulation was performed consisting of a heating phase from 50 K to 300 K with 2000 steps, followed by a cooling phase back to 50 K with 5000 steps. The energy threshold of van der Waals force was set to 50 K. In addition, the simulation results were further improved by running a short energy minimization comprising 500 steps of descent followed by 500 steps of conjugate gradient using an energy tolerance of 0.001 kcal/mol. It was considered as a failure when a docking did not have any output pose. Accuracy test was carried out by calculating the root mean square deviation (RMSD) after re-docking the internal ligand with the algorithm into the protein.

Behavioral tests

The Morris Water Maze test was carried out according to the previous description [22]. Initially, mice were given cued training for 3 days, and the position of the platform was marked using flag. Between different trials (four trials per day), the position of the platform and the orientation of the mouse being introduced into the pool were altered. The next day after the whole cued training, animals were given acquisition training for 6 days, and the triangular flag was taken away during this stage. During the whole training, the position of the platform remained static for every rodent sample, the trials were performed according to the operation of the cued training phase. Later, a probe trial was performed on the following day, during this stage, the platform was taken away, and every mouse was introduced from a novel entry point. The mouse then swam freely for 60 s, while the swimming track was recorded.

Step-down passive avoidance test (PA) was demonstrated to memory consolidation and memory retention studies. For the acclimation, mice were placed into the grid of step-down apparatus 24 h prior to the tests. The apparatus was a plastic box (30 cm × 30 cm × 40 cm high); the ground in the box consisted of parallel stainless steel bars (0.3 cm diameter spaced 1 cm apart). There was a Cylindrical plastic platform (5 cm × 5 cm × 5 cm) on the center of the grid floor. The test consisted of two parts: the training session and the retention session. During the training session, the animals were trained by placing them on the steel grids and then an electric shock was delivered to their paws *via* the rods of the grid floor (1 Hz, 0.5 s, 45 V DC) until they stepped up onto the platform. The time taken to jump onto the platform (reaction time) and the number of electric shocks they received were recorded. After 24 h, retention test session was performed, mice were placed on the steel grids, but not shocked, the latency to jump down into the steel ground in the dark chamber was recorded. 300 S was set as the max latency time [23, 24].

Novel object recognition test (NORT) was carried out in memory ability study. Animals were individually placed in a square cage and allowed to explore two identical objects placed in certain positions in the cage for 5 min (acclimation period). Then the cage was cleaned (to remove any scent), a novel object was put in to replace one of the two identical previous objects, and the mouse was then put back in the cage for another 5 min (test period). Time interacting with each object (nose within 1 cm of the object) was recorded. After 24 h, the test period was carried out, with the same original object but a different novel object. Values represent the percentage of time spent with the novel object *vs.* the total time spend with either object [25].

Golgi-Cox staining assay

Golgi-Cox staining was carried out with the FD Rapid Golgi Stain Kit (FD Neuro Technologies,

Columbia, MD, USA). Initially, mice were anesthetized then euthanized, the brains were dissected immediately and rinsed with PBS. The brains were then immerged in a mixture of FD Solution 1 (A:B = 1:1) for 14 days in darkness at room temperature, and then transferred to FD Solution C and kept at 4°C for 72 h in the dark. Solution C was changed after the first 24 h. 120 μm brain sections were cut using a Leica freezing microtome. Each section was mounted on gelatin-coated slides, and dried overnight. Then the sections were immerged in a mixture of FD Solution 2 (D:E:Milli-Q water = 1:1:2) for 10 min. After Milli-Q water washing, the slides were dehydrated in 50%, 70%, 95%, and pure alcohol and cleared in Xylene for 3 times, and coverslipped. Dendritic spine was imaged using an Olympus BX-51 microscope (Wetzlar, Germany).

Mouse primary neuron culture

Briefly described, the day 18 timed pregnant WT C57BL/6 mice were firstly anesthetized, and then the embryos were quickly removed from the uterus. Under sterile conditions, the embryonic brain was dissected and the cortical tissue was isolated. Carefully removed the dura mater and pia mater separately, then cut the cortical tissue into small pieces. After being cut into small pieces, 50 μL of 2.5% trypsin and 50 μL of 2 mg/mL DNase I were added into 1 mL minced tissue suspension in PBS and incubated at 37°C for 23 min. The digestion was terminated by adding FBS and centrifuged at 300 × g for 5 min at 4°C. The neurons were then resuspended in Neurobasal Medium (2% B27, 2 mM glutamine). The neuronal suspensions were subsequently plated on poly-D-lysine-coated 24-well plates. The cultures were maintained at 37°C with 5% CO_2. Replace half of the old medium with an equal amount of fresh medium once every three days. The cultures could be used for experiments on culture day 10. To induce cell injury, cells were incubated with 20 μM Aβ for 48 hours.

Cell viability analysis

Primary neurons were seeded in 96-well plates (3000 cells/well) and treated with the PTS at various concentrations (10^{-9} to 10^{-4} mol/L) or vehicle (0.1% DMSO). Cell viability was examined with a CellTiter 96® AQueous One Solution Cell proliferation assay (MTS) assay.

TUNEL staining

Terminal deoxynucleotidyl transferase-mediated dUTP-biotin nick end labeling (TUNEL) staining was performed using a TUNEL Apoptosis Assay Kit (solarbio, Beijing, China). Apoptotic cell nuclei were stained with fluorescein-dUTP, Hoechst was used to stain all cell nuclei. Briefly, the drug-treated primary neuron cells were fixed with paraformaldehyde for half an hour, gently rinsed with PBS, added with Triton-X-100 (0.2%) for 10 min at room temperature. Add the newly prepared TUNEL assay solution and incubate at 37°C in the dark for 1 h, observed using a fluorescence microscope.

Analysis of cAMP and cGMP concentrations

The primary neuron cells were maintained in Neurobasal Medium including 2% B27, 2 mM glutamine, cultured at 37°C in 5% CO_2. Cells were plated at 1×10^5 cells/well into 6-well plates for all the tests and were treated with different drugs for 24 h before tests [26]. After 24-hour treatment with PTS or rolipram, cells were treated with 0.1 M HCl containing 0.5% Triton X-100 and incubated for 10 min at room temperature. Then, the samples were centrifuged for 10 min (800 × g) to precipitate cellular debris. Cyclic AMP and cGMP were examined with Enzyme-linked immunosorbent assay (ELISA).

Western blot analysis

Briefly, primary neuron cells were lysed, then quantified proteins using the BCA assay. An equal amount of protein samples was subjected to SDS-PAG and electro-transferred to a 0.45 μm polyvinylidene difluoride membranes. The membranes were probed with primary antibodies as well as with a GAPDH antibody (1:3000) as a loading control. The membranes were then incubated with secondary antibody for 1 h followed with triple 10-min wash in TBS-T. Bands were visualized with an enhanced chemiluminescence (ECL) system. Data within a linear range were quantified using Quantity One software (BioRad).

Statistical analysis

All data are presented as the means ± SEM. Statistical analysis was conducted with SPSS 18.0 and GraphPad Prism 6.0. Multiple com-

Table 1. PTS exhibits higher score on druggable character-parameters than Resveratrol in TCMSP (Traditional Chinese Medicine System Pharmacology database)

Parameters	Pterostilbene	Resveratrol
Molecular Weight	256.32	228.26
BBB	0.49	0.18
DL evaluation	0.14	0.11
OB	77.54%	19.07%
Caco-2 permeability	1.20	0.80

Pterostilbene shows higher BBB score (the higher of the score, the easier to deliver through the blood brain barrier), higher drug like index score (the higher of the DL, the more probability of this molecule are developed into a market medicine.), higher oral bioavailability (OB) (the higher OB, the higher concentration of the original molecule in the blood) and higher Caco-2 permeability score (the higher of Caco-2 score means the molecule is the more permeable in intestine). All these data indicate Pterostilbene may be more a compound of more potential to be a market drug for Alzheimer's disease.

parisons among vehicle and treatment groups were operated by one-way ANOVA followed by Bonferroni correction. $P < 0.05$ was considered statistically significant.

Results

PTS presents more potential druggable characters than resveratrol

To identify the advantage of PTS' effect on memory deficit, four ADME standards in different parameters (BBB, DL, OB, and Caco-2 permeability) were used to compare PTS and Resveratrol (**Table 1**). As BBB is the first key factor on estimating a medicine against central neuro system disease. We found BBB index of PTS was 0.49, which was higher than the standard permeable index, as well as it was higher than BBB index of Resveratrol (0.18). In next step, assuring molecules with a high DL index could increase the possibility of therapeutic success, and the higher DL value a molecule had, the larger possibility it might possesses certain biological properties. $DL_{(PTS)}$ = 0.14 and $DL_{(Res)}$ = 0.11, both of them were lower than the system threshold of DL = 0.20. PTS exhibited more favorable DL features than Resveratrol. OB and Caco-2 permeability should also be assessed to ensure the reliability of screening model [27]. As a result, PTS exhibited proper oral bioavailability (OB = 77.54%), which was much higher than that of Resveratrol (OB = 19.07%). In addition, to evaluate the absorption property, we searched the Caco-2 permeability of PTS and Resveratrol. The results showed that PTS (Caco-2 = 1.20) was found meeting the threshold requirement of Caco-2 permeability (> -0.4).

Table 2. PTS shows higher interaction-energy score with PDE4A than with PDE2A or PDE4D in Docking simulation

Receptor	-CDOCKER INTERACTION ENERGY (kcal/mol)	
	Pterostilbene	Initial ligand
PDE2A	33.3183	52. 5304
PDE4A	36.926	39.643
PDE4D	35.907	50.034

The lower of the -CDOCKER INTERACTION ENERGY, the stronger affinity between Pterostilbene and the PDE protein.

PTS presents most potential affinity with PDE4A

As the screening-selected compound, PTS was docked with the potential targets. The CDOCKER INTERACTION ENERGY between PDE4A, PDE4D, PDE2A, and their initial ligands were shown in **Table 2**. The algorithm output told us PDE4A was simulated as the receptor of strongest affinity with PTS (-36.926 kcal/mol).

Figure 1A and **1B** displayed the 3D structure of PTS and Resveratrol. PTS molecule was displayed using a ball and stick model and the PDE4A protein was displayed using a macromolecular secondary structural model (**Figure 1C**). The 2D diagram simulation presented the OD1 in the ASP413 amino acid residue formed H-bonds with H35 of PTS. Pi-Sigma bond was detected between the ligand molecule PTS and HG11 in ILE548 amino acid residue of acceptor PDE4A, as well as a Pi-Pi conjugated bond between PTS and PHE584 residue of acceptor protein (**Figure 1D**). In next step, the best pose of PDE4A-PTS-complex from virtual screening and CDOCKER was selected, and the apo-form of protein (4W10) was subjected to 200 ns molecular dynamics (MD) simulations using Discovery Studio version 2.5. The stability of the protein was analyzed by H-bonds number (**Figure 1E**) and plotting root mean square deviation (RMSD) (**Figure 1F**). The RMSD plot of apo-form of protein and PDE4A-PTS-complex structure had shown deviation between 0.3 and 1.35 Å (**Figure 1F**). The Rg is also calculated to analyze the folding pattern of the protein during simulation [21] and is defined

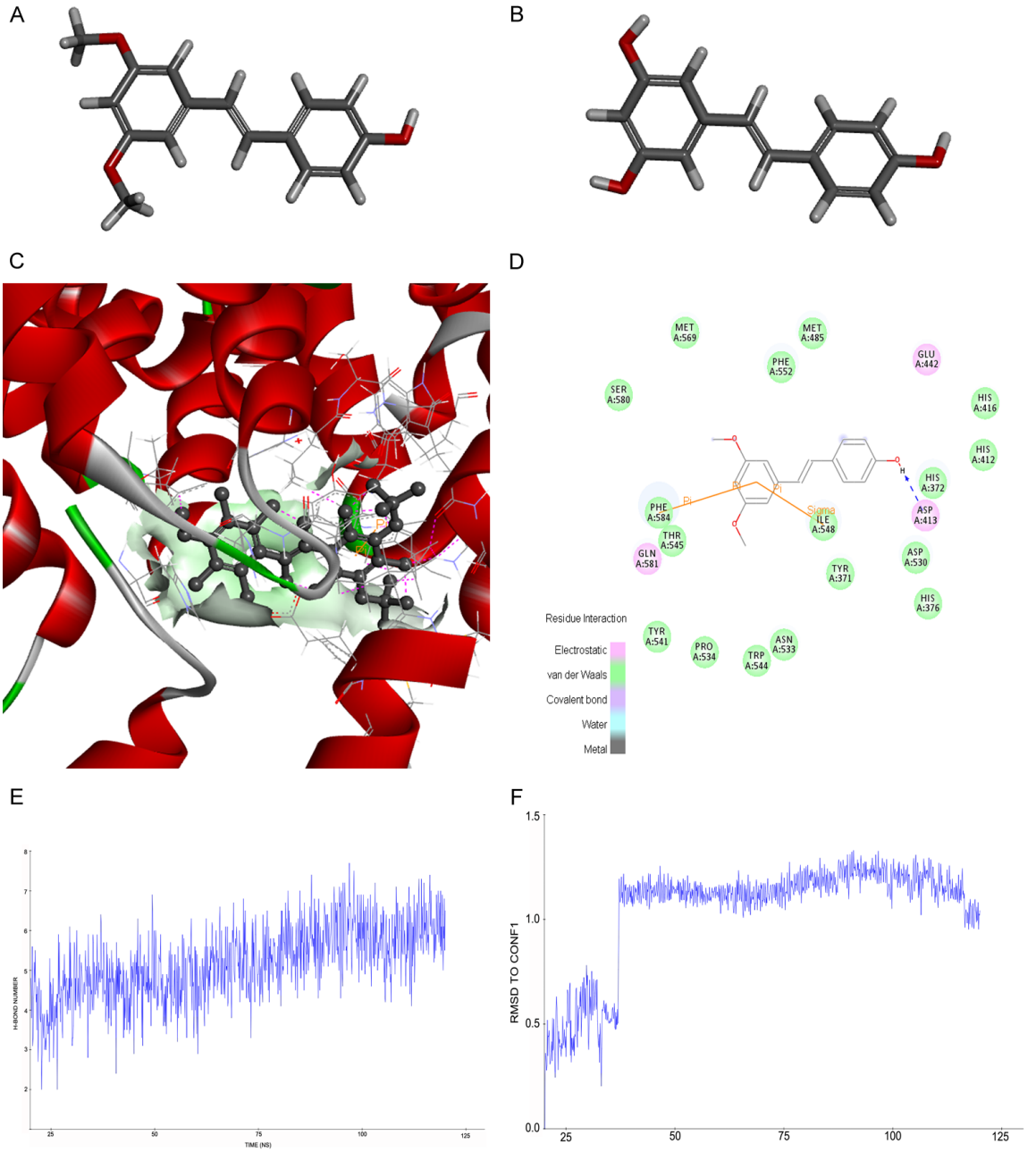

Figure 1. Molecular docking and molecular dynamics simulation between PTS and PDE4A protein using the CDOCKER algorithm. 3D structure of PTS (A) and Resveratrol (B). (C) The interaction residues and bonds in the PTS-PDE4A interaction. PTS molecule was displayed using a ball and stick model and the PDE4A protein was displayed using a macromolecular secondary structural model. (D) 2D-diagram interaction analysis between PTS and PDE4A. Change in the H-bond numbers (E) and the RMSD (F) in the 125 ns molecular dynamics simulation between PTS molecule and PDE4A receptor protein.

as the root mean square distance of the collection of atoms from their common center of gravity. The results of gyration showed not much deviation in the folding pattern of protein (data is not shown). The overall simulation of PDE4A-PTS-complex showed more stability (-12585.238 kcal/mol) than an apo-form of protein (-12438.166 kcal/mol) variation in energy parameters with respect to time and temperature.

PTS reverses memory impairment of APP/PS1 mice in rodent behavioral tests

To evaluate if PTS reversed memory impairment of transgenic AD model mice, we detect-

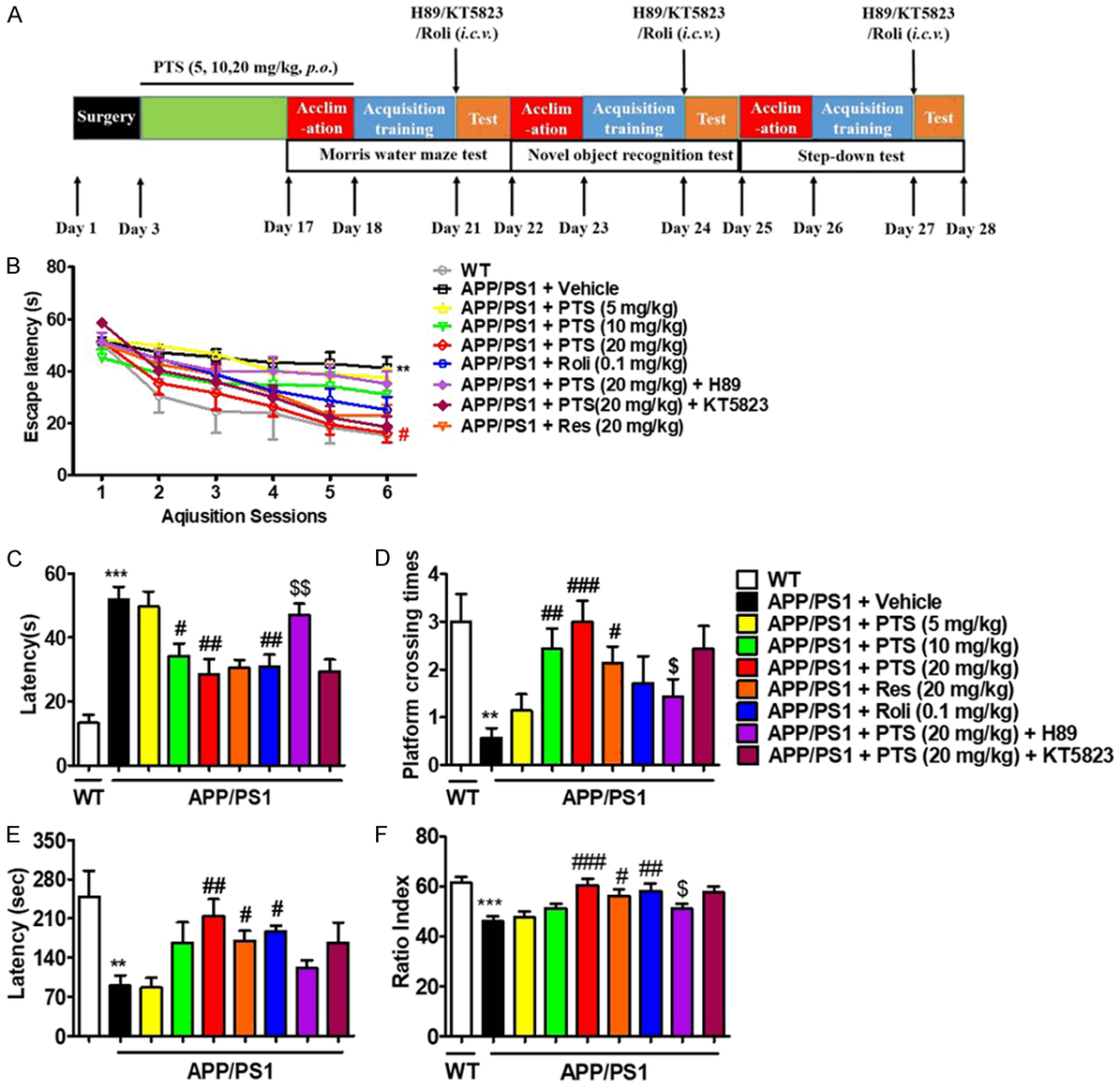

Figure 2. PTS-pretreatment (*p.o.*) reverses Aβ-induced memory impairment by behavioral test (MWM test, PA test and NORT). (A) Experimental timeline for drug treatments. (B) Learning curve in the MWM after treatment with PTS (mean ± SEM, n = 8 for each condition). $^{**}P < 0.01$, *vs.* WT mice group. $^{\#}P < 0.05$, *vs.* vehicle-treated APP/PS1 transgenic mice group. During the 24 h probe trails of the MWM task, the latency to get the platform (C), platform crossing time in the platform area (D) were tested after PTS treatment for 14 days (mean ± SEM, n = 8), as well as the retention in the PA test (E) and the ratio index in the NORT (F). $^{**}P < 0.01$, $^{***}P < 0.001$, *vs.* vehicle treated wild type mice group. $^{\#}P < 0.05$, $^{\#\#}P < 0.01$, $^{\#\#\#}P < 0.001$ *vs.* vehicle-treated APP/PS1 transgenic mice group. $^{\$}P < 0.05$, $^{\$\$}P < 0.05$, *vs.* PTS (20 mg/kg) treated APP/PS1 mice group. All the behavioral tests were performed 24 h after last drug treatment.

ed the mice memory performance in MWM and NORT in APP/PS1 transgenic mice treated with or without PTS at variant dosages (**Figure 2A**). After 6 blocks of acquisition training, all animals successfully located the platform, but the latencies to arrive the platform in groups are apparently different. Latencies to platform-reaching for PTS (20 mg/kg) treated AD model mice were significantly shorter than that of vehicle treated AD model mice ($P < 0.01$), which showed obvious longer latencies than vehicle treated control mice ($P < 0.01$) (**Figure 2B**). The 24 h memory retention for the platform location was observed on the probe trial. Compared to vehicle-treated group, PTS (10 mg/kg and 20 mg/kg) significantly shorten the elongation of latencies in AD model mice ($P < 0.05$, $P < 0.01$) (**Figure 2C**), as well as its apparently

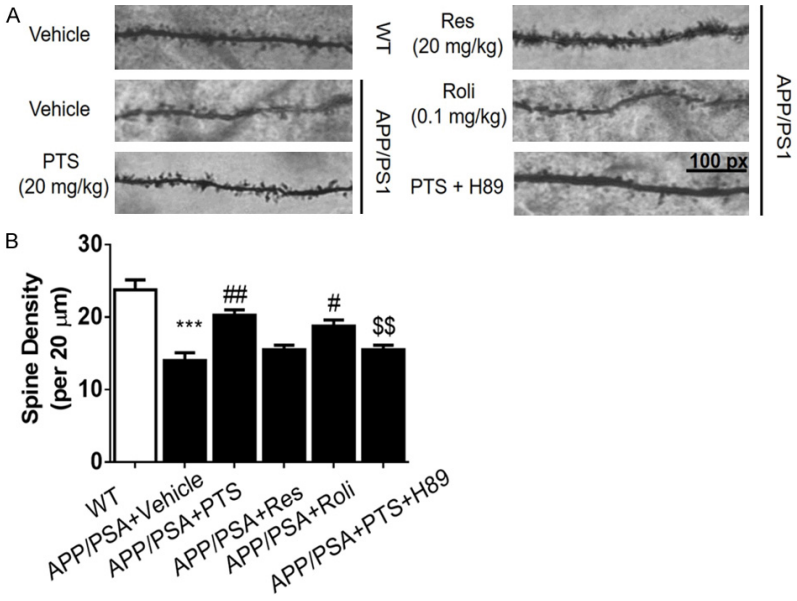

Figure 3. PTS (20 mg/kg) rescues the decrease in dendritic spine density in APP/PS1 mice based on Golgi-Cox staining. All three spine types can easily be seen following the Golgi staining. Staining was consistent across the entire length of the dendrite and the dendrite was isolated from other neurons. Representative photomicrograph of Golgi-Cox staining (A) and quantitative analysis results (B). Scale bar, 100 times magnification. $^{***}P < 0.001$, *vs.* vehicle treated wild type mice group. $^{\#}P < 0.05$, $^{\#\#}P < 0.01$, *vs.* vehicle-treated APP/PS1 transgenic mice group. $^{\$\$}P < 0.01$, *vs.* PTS (20 mg/kg) treated APP/PS1 mice group, n = 4.

reverse effects on the platform crossing number ($P < 0.01$, $P < 0.001$) (**Figure 2D**). Further, PKA inhibitor H89 blocked PTS's effects ($P < 0.05$), but PKG inhibitor KT5823 did not (**Figure 2C** and **2D**). As the positive control, selective PDE4 inhibitor Rolipram showed a significant change in the latency ($P < 0.01$) but not in platform crossing times.

We also confirmed PTS' effects with PA test. The animals were tested 24 h after acclimation, APP/PS1 transgenic AD model mice presented shorter latencies than vehicle treated control mice ($P < 0.01$). A dose-dependent elongation on latencies was observed in PTS treated groups, especially, the latency in PTS (20 mg/kg) treated mice was significantly longer than APP/PS1 mice ($P < 0.01$) (**Figure 2E**). As the positive control, selective PDE4 inhibitor Rolipram also showed a significant change in the latency ($P < 0.05$).

NORT was analyzed at 24 h after acclimation. Compared with the vehicle treated control group, APP/PS1 mice presented a remarkably lower ratio index ($P < 0.001$). Ratio index in PTS (20 mg/kg) treated group significantly ascended back to the same level as the vehicle treated control mice ($P < 0.001$). Besides, H89 blocked the reserve effect of PTS on NOR ratio index ($P < 0.05$), but KT5823 did not (**Figure 2F**).

PTS rescues the decrease in dendritic spine density in APP/PS1 mice

Synaptic failure is known to be one of the pathological processes of AD. We used Golgi-Cox staining to assess dendritic spine density (**Figure 3A**). The dendritic spine density in APP/PS1 mice was significantly reduced compared to wild type mice. While PTS (20 mg/kg) treatment significantly rescued the decrease in dendritic spine density ($P < 0.01$), and this effect was blocked by H89 (**Figure 3B**). A similar enhancing effect of Rolipram and Resveratrol on total dendritic spine in the hippocampal CA1 region was also noted in APP/PS1 mice. These findings suggest that PTS can alleviate hippocampal dendritic injury in APP/PS1 mice.

PTS protects primary neurons against Aβ-induced cell toxicity

Primary neurons were treated with PTS at different dosages for 24 h, as well as treated with 1×10^{-5} mol/L for different time spans, with or without being exposed to Aβ for 48 h. PTS (1×10^{-5} mol/L) obviously overcame Aβ-induced cells toxicity (**Figure 4C** and **4D**). As the positive control, Rolipram reversed Aβ-induced cell toxicity (**Figure 4C**). PTS 24 h treatment showed a remarkable reverse effect on Aβ-induced cell toxicity (**Figure 4D**). No significant effect was found when vehicle-treated cells were exposed to PTS (**Figure 4A** and **4B**).

PTS protects primary neuron cells against Aβ-induced apoptosis

Neuronal cell death is a major causal factor in the development of AD. We used TUNEL staining to detect apoptosis of primary neurons.

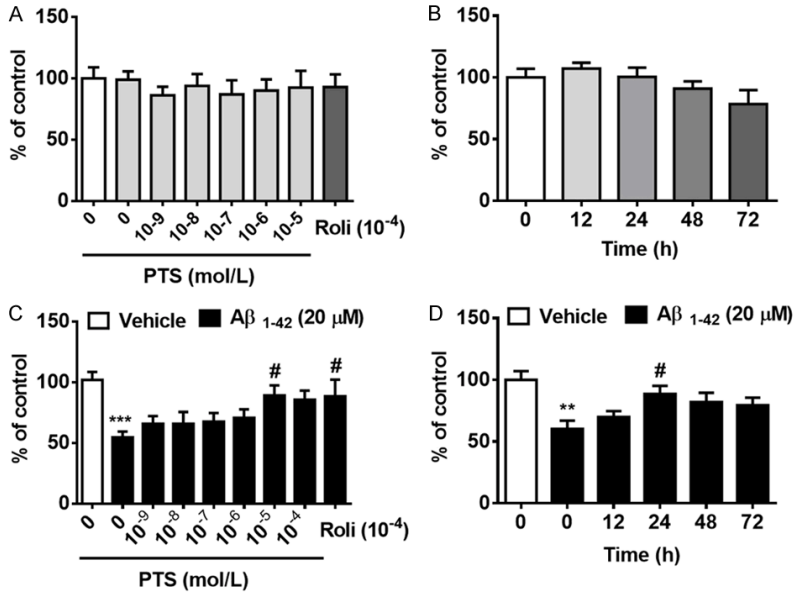

Figure 4. The effects of PTS on cell viability of primary neurons with or without Aβ-treated in dose-dependent and time dependent manners. Cell viability was measured by MTS assay. (A) PTS showed no-significant effect on the viability of primary neurons. The cells treated with the indicated concentrations of PTS for 24 h were assessed for viability via the MTS assay. The data represent the means ± SEM, n = 5. (B) No significant change in the viability with the time-dependent treatment of PTS. The effects of PTS on cell viability of Aβ-treated primary neurons in dose-dependent (C) and time dependent manners (D). Data represent mean ± SEM, $^{**}P < 0.01$, $^{***}P < 0.001$ vs. the non-Aβ-treated group (control). $^{\#}P < 0.05$ compared to the vehicle treated Aβ group.

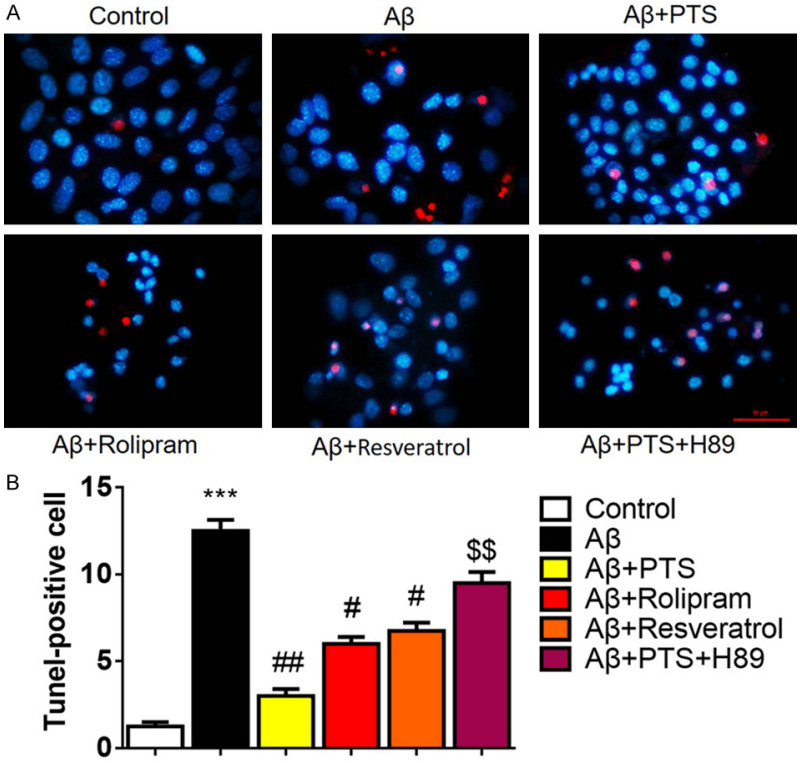

Figure 5. PTS (1×10^{-5} mol/L) protects against Aβ-induced apoptosis in primary neuron cells. The effect of PTS treatment on cell apoptosis was assessed by TUNEL staining in primary neuron cells. Representative images (A) and quantitative analysis results (B) of TUNEL staining. $^{***}P < 0.001$, *vs.* vehicle treated wild type mice group. $^{\#}P < 0.05$, $^{\#\#}P < 0.01$, *vs.* vehicle-treated Aβ group. $^{\$\$}P < 0.01$, *vs.* 1×10^{-5} mol/L PTS treated APP/PS1 mice group, n = 4.

TUNEL-positive cells, which were stained with red fluorescence, were not detected in the control group. Nuclei were stained by Hoechst with blue fluorescence (**Figure 5A**). After 20 μM Aβ exposure, apoptotic cells were markedly increased compared with the control group (**Figure 5B**). As expected, 1×10^{-5} mol/L PTS significantly reduced neurons apoptosis induced by Aβ ($P < 0.01$) (**Figure 5B**). As the positive control, Rolipram and Resveratrol also reduced the apoptosis of primary neuron cells. While treatment of PTS plus H89 failed to prevent neuronal death induced by Aβ, suggesting H89 blocks neuroprotective effect of PTS. These results, therefore, suggest that PTS protects neurons against apoptosis induced by Aβ.

PTS reverses Aβ-induced decreases in cAMP levels in primary neurons

The changes in cGMP and cAMP levels were detected after treatment with PTS in Aβ-exposed primary neuron cells. The significant decreases in cAMP and cGMP le-

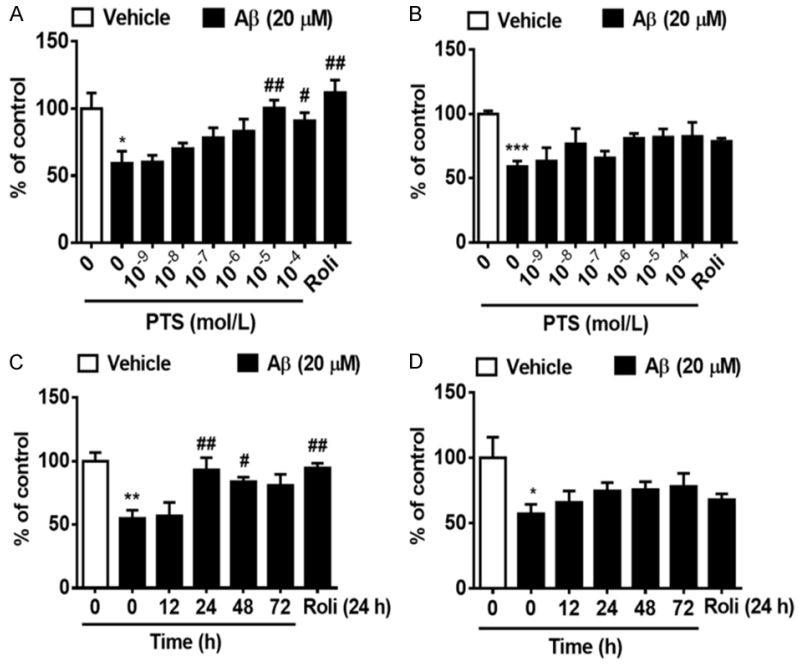

Figure 6. PTS reverses Aβ-induced decreases in cAMP levels, but not cGMP in primary neuron cells. ELISA analysis showed PTS reversed Aβ-induced cAMP (A and C) and cGMP (B and D) reduction in primary neuron cells in dose dependent (A and B) and time dependent (C and D) manners, respectively. The results represent the mean ± SEM, n = 5. $^{*}P < 0.05$, $^{**}P < 0.01$ and $^{***}P < 0.001$, compared vehicle-treated control group. $^{\#}P < 0.05$ and $^{\#\#}P < 0.01$, compared to vehicle-treated Aβ group.

vels were observed after Aβ exposure, and PTS (1×10^{-5} mol/L) treatment for 24 h increased cAMP level ($p < 0.01$) but not cGMP levels (**Figure 6A** and **6B**). Similarly, Rolipram increased the cAMP level but not cGMP. Besides, PTS (1×10^{-5} mol/L) treatment for 24 h can achieve the best effect (**Figure 6C** and **6D**).

PTS overcomes the effects of Aβ-induced decreased pVASP^{ser157}, pCREB and BDNF expression

To further confirm the PTS's effects on PDE4, we detected some of the down-stream proteins of PDE4/cAMP/VASP/CREB/BDNF signal pathway. As shown in **Figure 7A-E**, the ratio of phosphor-VASP^{ser157}/VASP and of pCREB/CREB were reduced by Aβ treatment ($P < 0.001$); while PTS partially blocked this effect at 20 μM for phosphor-VASP^{ser157}/VASP ($P < 0.001$) and 10 μM for pCREB/CREB ($P < 0.001$), indicating the regulation of PTS in the PDE-mediated cAMP/VASP/CREB signal pathway (**Figure 7B** and **7C**). We then analyzed BDNF expression with or without Aβ treatment or PTS treatment. BDNF expression was reduced by Aβ treatment ($P < 0.001$), while PTS blocked this reduction ($P < 0.001$) (**Figure 7D**). As the synaptic biomarker, PSD95 expression was decreased after Aβ treatment ($P < 0.001$) and was recovered when co-treated with PTS and Aβ ($P < 0.001$) (**Figure 7E**).

Discussion

Resveratrol's positive effects on alleviating AD have been widely reported [28]. In this study, we focused on a structural analog of Resveratrol, PTS, and its effects on APP/PS1 transgenic AD model *in vivo* and *in vitro*. With searching TCM-SP database, we found PTS was more druggable than Resveratrol according to its several druggable characters, such as BBB, DL, OB, and Caco-2 index. Furthermore, we illustrated PDE4A was the essential target of PTS, which protected primary neuron cells against Aβ-induced cytotoxicity.

Considering AD as a central nervous system disease, we firstly compared the BBB index between PTS and Resveratrol. PTS exhibited a much higher BBB index than Resveratrol, which meant a higher compound concentration in the brain. In the next step, we investigated the DL evaluation. DL evaluation is used to assess whether a compound is chemically suitable for being a drug, and how a drug-like molecule affect the parameters of their pharmacokinetic and pharmacodynamic properties which ultimately affecting their ADME properties [29]. In Wang's [30] recent work, they develop an *in silico* Model to forecast DL index of a compound, which is supported by a database of 6511 structurally diverse drugs and drug-like molecules from Drug Bank database. Based on these data, we calculated PTS's DL = 0.14, which was higher than that of Resveratrol. Furthermore, by observing OB and Caco-2 permeability, PTS performed higher OB index and

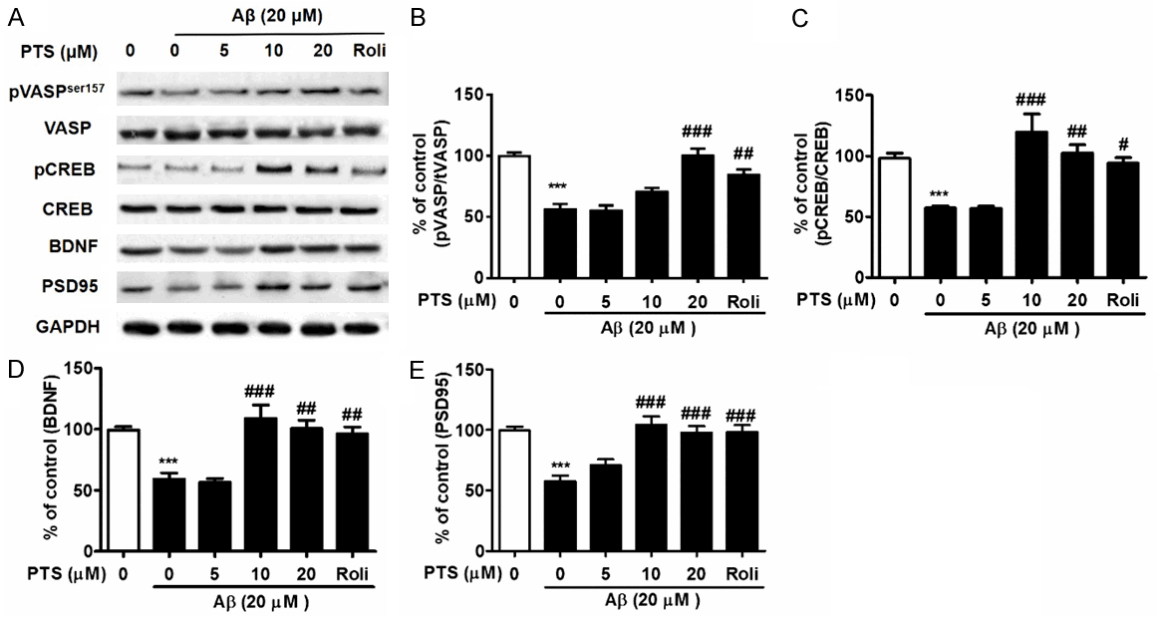

Figure 7. PTS overcomes the effects of Aβ-induced decreased pVASP^{ser157}, pCREB, BDNF, and PSD95 expression in primary neuron cells. Western blot analysis showed PTS (10, 20 μM) reversed Aβ-induced decrease expression of pVASP^{ser157}, pCREB, BDNF, and PSD95 expression in primary neuron cells (A). Bar charts show the quantification of pVASP (B), pCREB (C), BDNF (D) and PDS95 (E). The results represent the mean ± SEM, n = 3. ***p < 0.001, compared to vehicle-treated control group. ##p < 0.01 and ###p < 0.001, compared to vehicle-treated Aβ group.

Caco-2 permeability than Resveratrol (**Table 1**), which indicated PTS may present a more stable structure when it is orally administrated. In all of the four chosen pharmacodynamics and pharmacokinetic parameters, PTS showed higher scores than Resveratrol. This indicates that PTS may perform a higher efficiency on anti-Aβ-induced cytotoxicity.

As a classic AD animal model, APP/PS1 transgenic mice can partially reproduce memory deficit and neuropathological features in AD patients [31]. To assess the effectiveness of PTS in AD, the selective PDE4 inhibitor rolipram was used as a positive control treatment in behavioral testing. Consistent with proven results, Rolipram can alleviate cognitive deficits in APP/PS1 mice [32]. In this study, PTS-preventive treated APP/PS1 mice exhibited obvious improvement on learning-memory behaviors. At a dose of 20 mg/kg, PTS had a significant effect on all three sets of behavioral test.

Hippocampus is considered the main essential subregion during AD processing. Compared with other subtypes, changes in PDE4A and PDE4D levels were found in brains of early stage AD patients [33], as well as PDE2 enriches in hippocampus [34]. Therefore, we focused on PTS' regulation on function of PDE2 and two subtypes of PDE4. According to the Discovery Studio algorithm, the higher of -CDOCKER interaction energy, the higher of PTS and target acceptor infinity. The *in silico* simulation data pointed out the highest -CDOCKER interaction energy score of PTS and PDE4A, which presented the same level as the score of initial ligand and PDE4A interaction on its catalytic domain. For both PDE2 and PDE4D, the -CDOCKER interaction energy scores were both lower than that of initial ligand when docking the same acceptor. These results indicate that PDE4A may be the target of PDE with highest affinity to PTS in human brain. In addition, PTS formed H-bond with ASP413 residue, as well as its aromatic ring formed Pi-Pi and Pi-Sigma conjugated bonds with PHE584 and ILE548 residues, respectively. Zhao et al. compare PTS with its three analogs on their affinity with PDE4D with docking simulation assay and experimental binding assay [35]. Zhao's study supports our results, and we further discovered PTS's potential as an anti-neurotoxicity agent.

Despite the ligand-receptor affinity was not detected in this study, but as the substrate of PDE dehydration, cGMP and cAMP levels were

observed to test PTS inhibition of PDE catalysis. Aβ induced decrease in both cGMP and cAMP levels were partially reversed with PTS treatment. Vitolo. OV et al. have found that Aβ plagues reduce cAMP level by binding with a putative membrane receptor and inhibiting adenylate cyclase [36]. On the other hand, it is reported that Forskolin stimulating cAMP, also induce co-secretion of Aβ peptides with peptide and catecholamine neurotransmitters [37]. Regarding cAMP as a secondary messenger of involving in numerous signal pathway regulation, cell secretion of peptides and transmitters may be one of the downstream of cAMP-mediated signal pathways. PTS raised the cAMP level in a dose-dependent manner in Aβ treated cells. It provides evidence that PTS may elevate cAMP levels by inhibiting PDEs' function.

VASP is phosphorylated by PKA on serine 157 (Ser 157) [38]. We detected the changes in the downstream proteins of PDE/cAMP signal pathway. CREB phosphorylation at Ser133 is an important regulatory site by cGMP and VASP [39]. A lot of evidence indicates that Aβ treatment may interfere phosphorylation of CREB [40] and therefore blocking the expression of CRE-regulated genes such as BDNF in SH-SY5Y cells [41]. In this research, it was consistent with the previous studies which associated Aβ neurocytotoxicity with its effects on CREB/BDNF pathway. Evidence suggests that synaptic connections in the hippocampus and neocortex are lost in AD, and this loss is closely associated with decreased cognitive ability in AD patients [42]. Post synaptic density protein (PSD95) is localized at synapses, and its level is vital for function and structure of brain cells [43]. We discovered that PTS treatment reversed Aβ-induced decrease in PSD95 level. In Yang SF's study [44], they find that PTS treatment decreases nucleus-transportation of CREB, but effect of PTS on CREB expression has not been reported yet. Therefore, we not only illustrated that PTS protects primary neuron cells and APP/PS1 transgenic mice against Aβ-induced neurotoxicity, but revealed this effect was involved in direct binding of PTS on PDE4A and in regulating the PDE/cyclic-AMP/CREB/BDNF signaling pathway, which lead to synaptic junction recovery.

Acknowledgements

This work was supported by the Shaanxi Fourth People's Hospital (No. 2017SY-004). Discovery Studio (DS) 2.5 was provided by Liangren Zhang, we are very grateful for software supporting.

Disclosure of conflict of interest

None.

Address correspondence to: Dr. Wei Liu, Department of Medical Science Research Center, Shaanxi Fourth People's Hospital, 512, East XianNing Road, Xi'an 710043, China. Tel: +86 29 89531040; Fax: +86 29 89531040; E-mail: vincelau@sina.com

References

[1] Larson EB, Kukull WA and Katzman RL. Cognitive impairment: dementia and Alzheimer's disease. Annu Rev Public Health 1992; 13: 431-449.

[2] Harrison JR and Owen MJ. Alzheimer's disease: the amyloid hypothesis on trial. Br J Psychiatry 2016; 208: 1-3.

[3] Nthenge-Ngumbau DN and Mohanakumar KP. Can cyclic nucleotide phosphodiesterase inhibitors be drugs for Parkinson's disease? Mol Neurobiol 2018; 55: 822-834.

[4] Heckman PR, Wouters C and Prickaerts J. Phosphodiesterase inhibitors as a target for cognition enhancement in aging and Alzheimer's disease: a translational overview. Curr Pharm Des 2015; 21: 317-331.

[5] Bollen E and Prickaerts J. Phosphodiesterases in neurodegenerative disorders. IUBMB Life 2012; 64: 965-970.

[6] Wang ZZ, Zhang Y, Zhang HT and Li YF. Phosphodiesterase: an interface connecting cognitive deficits to neuropsychiatric and neurodegenerative diseases. Curr Pharm Des 2015; 21: 303-316.

[7] Sierksma AS, Rutten K, Sydlik S, Rostamian S, Steinbusch HW, van den Hove DL and Prickaerts J. Chronic phosphodiesterase type 2 inhibition improves memory in the APPswe/PS1dE9 mouse model of Alzheimer's disease. Neuropharmacology 2013; 64: 124-136.

[8] Francis SH, Blount MA and Corbin JD. Mammalian cyclic nucleotide phosphodiesterases: molecular mechanisms and physiological functions. Physiol Rev 2011; 91: 651-690.

[9] Cui Q and So KF. Involvement of cAMP in neuronal survival and axonal regeneration. Anat Sci Int 2004; 79: 209-212.

[10] Lu YF and Hawkins RD. Ryanodine receptors contribute to cGMP-induced late-phase LTP and CREB phosphorylation in the hippocampus. J Neurophysiol 2002; 88: 1270-1278.

[11] Merz K, Herold S and Lie DC. CREB in adult neurogenesis--master and partner in the de-

velopment of adult-born neurons? Eur J Neurosci 2011; 33: 1078-1086.
[12] Meyer-Franke A, Wilkinson GA, Kruttgen A, Hu M, Munro E, Hanson MG Jr, Reichardt LF and Barres BA. Depolarization and cAMP elevation rapidly recruit TrkB to the plasma membrane of CNS neurons. Neuron 1998; 21: 681-693.
[13] Perez-Torres S, Cortes R, Tolnay M, Probst A, Palacios JM and Mengod G. Alterations on phosphodiesterase type 7 and 8 isozyme mRNA expression in Alzheimer's disease brains examined by in situ hybridization. Exp Neurol 2003; 182: 322-334.
[14] Ma T, Tan MS, Yu JT and Tan L. Resveratrol as a therapeutic agent for Alzheimer's disease. Biomed Res Int 2014; 2014: 350516.
[15] Casadesus G, Shukitt-Hale B, Stellwagen HM, Zhu X, Lee HG, Smith MA and Joseph JA. Modulation of hippocampal plasticity and cognitive behavior by short-term blueberry supplementation in aged rats. Nutr Neurosci 2004; 7: 309-316.
[16] Chang J, Rimando A, Pallas M, Camins A, Porquet D, Reeves J, Shukitt-Hale B, Smith MA, Joseph JA and Casadesus G. Low-dose pterostilbene, but not resveratrol, is a potent neuromodulator in aging and Alzheimer's disease. Neurobiol Aging 2012; 33: 2062-2071.
[17] Li Y, Qiang X, Li Y, Yang X, Luo L, Xiao G, Cao Z, Tan Z and Deng Y. Pterostilbene-O-acetamidoalkylbenzylamines derivatives as novel dual inhibitors of cholinesterase with anti-beta-amyloid aggregation and antioxidant properties for the treatment of Alzheimer's disease. Bioorg Med Chem Lett 2016; 26: 2035-2039.
[18] Fu Z, Yang J, Wei Y and Li J. Effects of piceatannol and pterostilbene against beta-amyloid-induced apoptosis on the PI3K/Akt/Bad signaling pathway in PC12 cells. Food Funct 2016; 7: 1014-1023.
[19] Puzzo D, Gulisano W, Palmeri A and Arancio O. Rodent models for Alzheimer's disease drug discovery. Expert Opin Drug Discov 2015; 10: 703-711.
[20] Xu X, Zhang W, Huang C, Li Y, Yu H, Wang Y, Duan J and Ling Y. A novel chemometric method for the prediction of human oral bioavailability. Int J Mol Sci 2012; 13: 6964-6982.
[21] Xiaokaiti Y, Wu H, Chen Y, Yang H, Duan J, Li X, Pan Y, Tie L, Zhang L and Li X. EGCG reverses human neutrophil elastase-induced migration in A549 cells by directly binding to HNE and by regulating alpha1-AT. Sci Rep 2015; 5: 11494.
[22] Bouter Y, Kacprowski T, Weissmann R, Dietrich K, Borgers H, Brauss A, Sperling C, Wirths O, Albrecht M, Jensen LR, Kuss AW and Bayer TA. Deciphering the molecular profile of plaques, memory decline and neuron loss in two mouse models for Alzheimer's disease by deep sequencing. Front Aging Neurosci 2014; 6: 75.
[23] Jafari-Sabet M and Jannat-Dastjerdi I. Muscimol state-dependent memory: involvement of dorsal hippocampal mu-opioid receptors. Behav Brain Res 2009; 202: 5-10.
[24] Jafari-Sabet M. Involvement of dorsal hippocampal muscarinic cholinergic receptors on muscimol state-dependent memory of passive avoidance in mice. Life Sci 2011; 88: 1136-1141.
[25] Zhang RS, Xu HJ, Jiang JH, Han RW, Chang M, Peng YL, Wang Y and Wang R. Endomorphin-1 attenuates Abeta42 induced impairment of novel object and object location recognition tasks in mice. Brain Res 2015; 1629: 210-220.
[26] Schuster C, Williams LM, Morris A, Morgan PJ and Barrett P. The human MT1 melatonin receptor stimulates cAMP production in the human neuroblastoma cell line SH-SY5Y cells via a calcium-calmodulin signal transduction pathway. J Neuroendocrinol 2005; 17: 170-178.
[27] Muegge I. Selection criteria for drug-like compounds. Med Res Rev 2003; 23: 302-321.
[28] Sarubbo F, Moranta D, Asensio VJ, Miralles A and Esteban S. Effects of resveratrol and other polyphenols on the most common brain age-related diseases. Curr Med Chem 2017; 24: 4245-4266.
[29] Walters WP and Murcko MA. Prediction of 'drug-likeness'. Adv Drug Deliv Rev 2002; 54: 255-271.
[30] Ru J, Li P, Wang J, Zhou W, Li B, Huang C, Li P, Guo Z, Tao W, Yang Y, Xu X, Li Y, Wang Y and Yang L. TCMSP: a database of systems pharmacology for drug discovery from herbal medicines. J Cheminform 2014; 6: 13.
[31] Garcia-Alloza M, Robbins EM, Zhang-Nunes SX, Purcell SM, Betensky RA, Raju S, Prada C, Greenberg SM, Bacskai BJ and Frosch MP. Characterization of amyloid deposition in the APPswe/PS1dE9 mouse model of Alzheimer disease. Neurobiol Dis 2006; 24: 516-524.
[32] Guo H, Cheng Y, Wang C, Wu J, Zou Z, Niu B, Yu H, Wang H and Xu J. FFPM, a PDE4 inhibitor, reverses learning and memory deficits in APP/PS1 transgenic mice via cAMP/PKA/CREB signaling and anti-inflammatory effects. Neuropharmacology 2017; 116: 260-269.
[33] Perez-Torres S, Miro X, Palacios JM, Cortes R, Puigdomenech P and Mengod G. Phosphodiesterase type 4 isozymes expression in human brain examined by in situ hybridization histochemistry and [3H] rolipram binding autoradiography. Comparison with monkey and rat brain. J Chem Neuroanat 2000; 20: 349-374.
[34] Lakics V, Karran EH and Boess FG. Quantitative comparison of phosphodiesterase mRNA distribution in human brain and peripheral tissues. Neuropharmacology 2010; 59: 367-374.

[35] Zhao P, Chen SK, Cai YH, Lu X, Li Z, Cheng YK, Zhang C, Hu X, He X and Luo HB. The molecular basis for the inhibition of phosphodiesterase-4D by three natural resveratrol analogs. Isolation, molecular docking, molecular dynamics simulations, binding free energy, and bioassay. Biochim Biophys Acta 2013; 1834: 2089-2096.

[36] Vitolo OV, Sant'Angelo A, Costanzo V, Battaglia F, Arancio O and Shelanski M. Amyloid beta-peptide inhibition of the PKA/CREB pathway and long-term potentiation: reversibility by drugs that enhance cAMP signaling. Proc Natl Acad Sci U S A 2002; 99: 13217-13221.

[37] Toneff T, Funkelstein L, Mosier C, Abagyan A, Ziegler M and Hook V. Beta-amyloid peptides undergo regulated co-secretion with neuropeptide and catecholamine neurotransmitters. Peptides 2013; 46: 126-135.

[38] Eckert RE and Jones SL. Regulation of VASP serine 157 phosphorylation in human neutrophils after stimulation by a chemoattractant. J Leukoc Biol 2007; 82: 1311-1321.

[39] Lueptow LM, Zhan CG and O'Donnell JM. Cyclic GMP-mediated memory enhancement in the object recognition test by inhibitors of phosphodiesterase-2 in mice. Psychopharmacology (Berl) 2016; 233: 447-456.

[40] Oguchi T, Ono R, Tsuji M, Shozawa H, Somei M, Inagaki M, Mori Y, Yasumoto T, Ono K and Kiuchi Y. Cilostazol suppresses abeta-induced neurotoxicity in SH-SY5Y cells through inhibition of oxidative stress and MAPK signaling pathway. Front Aging Neurosci 2017; 9: 337.

[41] Garzon DJ and Fahnestock M. Oligomeric amyloid decreases basal levels of brain-derived neurotrophic factor (BDNF) mRNA via specific downregulation of BDNF transcripts IV and V in differentiated human neuroblastoma cells. J Neurosci 2007; 27: 2628-2635.

[42] Sultana R, Banks WA and Butterfield DA. Decreased levels of PSD95 and two associated proteins and increased levels of BCl2 and caspase 3 in hippocampus from subjects with amnestic mild cognitive impairment: insights into their potential roles for loss of synapses and memory, accumulation of Abeta, and neurodegeneration in a prodromal stage of Alzheimer's disease. J Neurosci Res 2010; 88: 469-477.

[43] Martin AM, Kuhlmann C, Trossbach S, Jaeger S, Waldron E, Roebroek A, Luhmann HJ, Laatsch A, Weggen S, Lessmann V and Pietrzik CU. The functional role of the second NPXY motif of the LRP1 beta-chain in tissue-type plasminogen activator-mediated activation of N-methyl-D-aspartate receptors. J Biol Chem 2008; 283: 12004-12013.

[44] Lin CW, Chou YE, Chiou HL, Chen MK, Yang WE, Hsieh MJ and Yang SF. Pterostilbene suppresses oral cancer cell invasion by inhibiting MMP-2 expression. Expert Opin Ther Targets 2014; 18: 1109-1120.